# Choosing Physics Constraints for Neural ODE Reactor Surrogates

**Tubhyam Karthikeyan**
Department of Chemical Engineering
Institute of Chemical Technology, Mumbai
tubhyam@ictmumbai.edu.in

## Abstract

Neural ODE surrogates for chemical reactors can violate fundamental physical laws—producing negative concentrations, non-conserving mass, and physically impossible trajectories that compound into surrogate collapse on long rollout horizons. We present a comparative study of physics-enforcing inductive biases: soft $\ell_2$ penalty methods, post-solve feasibility maps ("hard enforcement"), and architectural state reparameterisations (log-space, stoichiometric-rate) evaluated on three canonical reactor benchmarks. *Inductive bias scope determines both safety and accuracy*: soft penalties produce seed-dependent violations (0–41%) that persist across all $\lambda$ and training budgets tested (up to $\lambda = 100$, 500 epochs). Hard post-solve enforcement is the robust safe default for mixed or unknown state structure (0.00% violations, 99% NMSE reduction on exothermic CSTR), but log-parameterisation dominates on all-concentration states ($600\times$ better on VDV CSTR) while failing catastrophically on mixed states ($\mathrm{NMSE} = 10^4$). Code: `reactor-twin` on PyPI.

## 1 Introduction

Production-grade CSTR simulations require $\mathcal{O}(10^3)$ solver evaluations per second of process time, constraining real-time deployment in model predictive control, state estimation, and digital-twin applications. Neural ODEs [Chen et al., 2018] replace the mechanistic right-hand side with a learned function $f_\theta(z, t)$, achieving 11–19$\times$ CPU speedup over adaptive solvers (19$\times$/16$\times$/11$\times$ on exothermic/VDV/batch vs. `scipy` LSODA at $\mathrm{rtol} = 10^{-7}$). ChemNODE [Owoyele and Pal, 2022] and Phy-ChemNODE [Sharma et al., 2023] demonstrate strong accuracy on CSTR benchmarks, but share a fundamental flaw.

**The violation problem.** The unconstrained MLP $f_\theta$ has no mechanism preventing physically impossible trajectories. Concentrations become negative; mass is not conserved; temperature evolves outside physically permissible bounds. Constraint drift compounds over rollouts; without conservation invariants, long-horizon simulation can diverge qualitatively. Negative concentrations cause log-domain failures in downstream thermodynamics modules; mass non-conservation drives EKF filter divergence. Our experiments confirm this: unconstrained models incur 41% positivity violations and mass drift $0.021 \pm 0.011$ on standard benchmarks (Table 1).

**Why soft penalties fail.** Adding $\lambda\mathcal{V}(z)$ to the training loss creates a *training–inference gap*: at deployment no penalty fires, so constraint satisfaction is an accident of optimisation. Three seeds on the same benchmark at $\lambda = 1$ produce violation rates of 0%, 16%, and 38%—a 38 percentage-point range (Figure 1(e)). No $\lambda$ closes the gap: at $\lambda = 100$ the mean rate is still 3.7%, with MSE 81% higher than hard post-solve enforcement (Figure 1(c–d)).

38th Conference on Neural Information Processing Systems (NeurIPS 2024).

**This work.** We enforce constraints via post-solve enforcement—after `odeint` returns trajectory $z(t)$, a differentiable map $\tilde{z} = g(z)$ satisfies the constraint at every output point—and compare it systematically against soft penalties and architectural reparameterisations on matched benchmarks. The key finding: *no single method dominates across state structures*, but the choice is principled and can be made from state-structure inspection alone.

**Contributions.** (1) A composable framework of seven physics constraint modules, released as `reactor-twin` on PyPI. (2) Empirical evidence that soft $\ell_2$ penalty violations persist across seeds and two orders of magnitude of $\lambda$ ($\lambda = 1$–$100$, 500 epochs). (3) A comparative study establishing that accuracy depends on whether the structural assumption spans the full state: use hard enforcement for mixed or unknown state structure, log-param for all-concentration states, stoich-param for reaction-explicit systems.

## 2 Background

A Neural ODE [Chen et al., 2018] defines dynamics $\dot{z} = f_\theta(z, t)$ integrated by a differentiable solver:

$$z(t_1) = z(t_0) + \int_{t_0}^{t_1} f_\theta\big(z(t), t\big)\,\mathrm{d}t. \tag{1}$$

Gradients $\partial\mathcal{L}/\partial\theta$ are computed via the adjoint at $\mathcal{O}(1)$ memory cost. The function $f_\theta$ is an unconstrained MLP; nothing prevents it from producing $\dot{z}$ that integrate to unphysical $z(t)$.

PINNs [Raissi et al., 2019] augment the loss with physics residuals but share the training–inference gap. Hamiltonian [Greydanus et al., 2019] and Lagrangian [Cranmer et al., 2020] NNs give exact conservation but only for symplectic or Euler–Lagrange structure—not the heterogeneous constraints of chemical reactors. Finzi et al. [Finzi et al., 2020] enforce constraints via explicit projection layers (closest prior to our hard enforcement, but limited to classical mechanics structure); see Kidger [2022] for a general survey. ChemNODE [Owoyele and Pal, 2022] and PhyChemNODE [Sharma et al., 2023] apply soft penalties to CSTRs; both share the training–inference gap.

## 3 Method: Constraint Framework

Each physics constraint is an `AbstractConstraint` module:

$$\texttt{forward}(z) \;\to\; (\tilde{z},\; v), \tag{2}$$

where $\tilde{z}$ is the corrected (feasible) state and $v \geq 0$ is a scalar violation. In *hard mode*, $\tilde{z} = g(z)$ and $v = 0$; the data loss $\mathcal{L}$ trains $f_\theta$ with gradients flowing through $g$. In *soft mode*, $\tilde{z} = z$ and $v = \mathcal{V}(z)$; the total physics loss $\mathcal{L}_{\text{phys}} = \sum_i w_i v_i$ augments the data loss. Constraints compose as a sequential `ConstraintPipeline` applied after each `odeint` call.

### 3.1 Mass Balance Projection

For a reactor with stoichiometric matrix $S \in \mathbb{R}^{n_r \times n_s}$, all realisable concentration changes lie in $\mathrm{range}(S^\top)$. The orthogonal projection onto this subspace is:

$$P_{\text{mass}} = S^\top (S S^\top)^\dagger S \;\in\; \mathbb{R}^{n_s \times n_s}, \tag{3}$$

where $\dagger$ denotes the Moore–Penrose pseudoinverse (equal to the ordinary inverse when $S$ has full row rank; handles dependent reactions without modification); $P_{\text{mass}}$ is symmetric, idempotent, rank-$\mathrm{rank}(S)$. The corrected trajectory is $\tilde{C}(t) = C(t_0) + P_{\text{mass}}\,\Delta C(t)$, satisfying $(I - P_{\text{mass}})\Delta C = 0$ exactly. The Jacobian of $P_{\text{mass}}$ is itself (a constant linear map), so gradients flow without attenuation.

### 3.2 Positivity Feasibility Map

For concentration positivity we use a smooth feasibility map—not an orthogonal projection:

$$\tilde{z}_i = \log(1 + \exp(z_i)) + \varepsilon, \quad \varepsilon = 10^{-6}, \tag{4}$$

applied element-wise to species dimensions. The Jacobian $\partial\tilde{z}_i/\partial z_i = \sigma(z_i) \in (0,1)$ is differentiable everywhere (unlike ReLU) with bounded derivative in $(0,1)$; $\sigma(z_i) \to 0$ for large negative $z_i$, so gradient flow through $g$ weakens when $f_\theta$ produces strongly negative outputs early in training, mitigated here by gradient clipping (clip 5.0). Unlike Eq. (3), this is not a Euclidean projection: it shifts states away from zero rather than mapping to the nearest feasible point. When composed after mass balance (the correct ordering), the total mass is $C_{\text{total}} + n_s\varepsilon$—a deterministic, known offset. Both guarantees hold at every discrete output time point; inter-step satisfaction depends on solver step size.

# 4 Experiments

## 4.1 Benchmarks and Setup

**Three benchmarks.** *Exothermic CSTR*: $A \to B$ with heat integration and steady-state multiplicity; state $(C_A, C_B, T)$; constraint: positivity on $(C_A, C_B)$. *Van de Vusse (VDV) CSTR*: $A \to B \to C$, $2A \to D$ in a CSTR [Van de Vusse, 1964]; state $(C_A, C_B, C_C, C_D)$; constraint: positivity. *Batch* $A \to B \to C$: consecutive first-order in a closed batch; state $(C_A, C_B, C_C)$; constraint: mass balance $(\sum_i C_i = \text{const})$.

**Architecture and training.** All models: NeuralODE, 3-layer MLP ($d = 64$), tanh, RK4 ($\sim$14 K parameters). Adam with cosine annealing, 200 epochs (main ablation), gradient clip 5.0; 500 epochs for convergence study (§4.3). Data: 24 train and 8 val trajectories; $\pm 40\%$ concentration and $\pm 15$ K perturbations around steady state. Three seeds (42, 43, 44); results reported as mean $\pm$ std.

**Seven conditions.** (1) *None*: unconstrained. (2–3) *Soft* $\lambda \in \{1, 10\}$: $\ell_2$ penalty. (4) *Hard*: post-solve enforcement, gradients flow through $g$. (5) *Log-param*: concentrations in log-space; temperature stays linear for exothermic CSTR (mixed state). (6) *Stoich-param* (batch only): ODE outputs rates $r$; $\mathrm{d}C/\mathrm{d}t = S^\top r$. (7) *Hard (IO)*: trained unconstrained, projection at inference only. Training loss is computed in each condition's native parameterisation; NMSE is always in physical space (log-param models mapped back via $\exp(\cdot)$ before Eq. (5)).

**Metrics.** Violation: positivity fraction (%) for CSTRs; mass drift $|\Delta\sum_i C_i|$ for batch; also min-concentration and integrated negativity (both zero when no violation occurs). Long-rollout accuracy:

$$\text{NMSE} = \frac{1}{d}\sum_{k=1}^{d} \frac{\left\|z_k - \hat{z}_k\right\|^2}{\max\left(\bar{z}_k,\ 10^{-2}\right)^2}, \qquad \bar{z}_k = \mathbb{E}_{t,b}\big[|z_k|\big]. \tag{5}$$

Per-dimension normalisation makes NMSE scale-invariant across concentrations ($\sim$0.5 mol/L) and temperature ($\sim$350 K). Pre-projection drift $\delta = \|z(t) - g(z(t))\|/\|z(t)\|$ measures the relative correction applied by the full feasibility pipeline $g(\cdot)$ (distinct from $P_{\text{mass}}$) at evaluation; larger $\delta$ indicates the raw model output is farther from the feasible set.

## 4.2 Main Ablation

Table 1 gives the full results. All hard-mode conditions achieve $\mathbf{0.00\%} \pm \mathbf{0.00\%}$ violations by construction. Soft penalties show persistent, seed-dependent violations at every $\lambda$.

**Hard post-solve enforcement.** On **exothermic CSTR**, hard achieves 0.711 NMSE vs. 93.2 unconstrained (99% reduction); the model actively leverages $g$ as a corrective element during training (pre-projection drift $= 0.825$, indicating $g$ resolves large deviations before the loss is computed). On **VDV CSTR**, hard (softplus) degrades to 246.5 (165.3 unconstrained): per-species shifts disrupt stoichiometric coupling for species C and D near zero; substituting ReLU projection (104.3, 0.00%) confirms the cost is map-specific (ReLU restricted to VDV: exo CSTR drift $= 0.825$ warrants smooth softplus). On **batch**, a modest improvement (0.431 vs. 0.494).

**Architectural baselines.** Log-param is $600\times$ better than hard on VDV (0.272 vs. 246.5): uniform log-space preserves stoichiometric ratios. It fails catastrophically on exothermic CSTR ($10^4$): the mixed state $[\log C_A, \log C_B, T]$ creates gradient scale mismatch—$\mathrm{d}(\log C_A)/\mathrm{d}t \sim 1/C_A$ blows up near the minimum while $\mathrm{d}T/\mathrm{d}t$ stays moderate. Stoich-param is $17\times$ better than hard on batch (0.026 vs. 0.431): $\mathrm{d}C/\mathrm{d}t = S^\top r$ matches physical structure exactly.

Table 1: Full ablation over 3 seeds (42, 43, 44). NMSE: long-rollout (Eq. 5). Violation: positivity fraction (%) for CSTRs; mean mass drift for batch. *Hard*: post-solve enforcement at training and inference. *Hard (IO)*: enforcement at inference only. *Log*/*Stoich*: architectural baselines. **Bold**: lowest violation. †: lowest NMSE per system. For all conditions reporting **0.00%** violations, min-concentration and integrated negativity are likewise zero by construction.

| System | Condition | NMSE ↓ | | Violation ↓ | |
|---|---|---|---|---|---|
| | | Mean | Std | Mean | Std |
| Exo CSTR | None | 93.20 | 57.66 | 41.0% | 8.3% |
| | Soft ($\lambda=1$) | 5.71 | 2.64 | 17.9% | 19.1% |
| | Soft ($\lambda=10$) | 30.91 | 37.88 | 7.1% | 12.3% |
| | **Hard**† | **0.711** | **0.000** | **0.00%** | **0.00%** |
| | Log-param | 10106 | 6529 | **0.00%** | 0.00% |
| | Hard (IO) | 42.22 | 47.46 | **0.00%** | 0.00% |
| VDV CSTR | None | 165.3 | 78.6 | 14.0% | 13.9% |
| | Soft ($\lambda=1$) | 173.5 | 70.3 | 4.1% | 0.3% |
| | Soft ($\lambda=10$) | 186.4 | 60.5 | 1.9% | 0.1% |
| | **Hard** | 246.5 | 69.4 | **0.00%** | 0.00% |
| | **Hard (ReLU)** | 104.3 | 86.2 | **0.00%** | 0.00% |
| | Log-param† | **0.272** | **0.219** | **0.00%** | 0.00% |
| | Hard (IO) | 2926 | 443 | **0.00%** | 0.00% |
| Batch $A\to B\to C$ | None | 0.494 | 0.113 | $2.11\times10^{-2}$ | $1.09\times10^{-2}$ |
| | Soft ($\lambda=1$) | 0.610 | 0.065 | $1.81\times10^{-2}$ | $1.57\times10^{-2}$ |
| | Soft ($\lambda=10$) | 1.028 | 0.267 | $1.50\times10^{-2}$ | $1.32\times10^{-2}$ |
| | **Hard** | 0.431 | 0.124 | $4.95\times10^{-8}$ | $1.67\times10^{-8}$ |
| | Stoich† | **0.026** | **0.029** | $\mathbf{7.57\times10^{-8}}$ | $\mathbf{1.57\times10^{-8}}$ |
| | Hard (IO) | 0.477 | 0.130 | $3.33\times10^{-8}$ | $3.10\times10^{-10}$ |

**Training regularisation vs. inference correction.** Applying enforcement only at inference (*Hard (IO)*): on exothermic CSTR (drift $= 0.003$) it reduces NMSE from $93.2$ to $42.2$, but falls far short of full hard ($0.711$); on VDV (drift $= 0.537$), inference enforcement is catastrophic ($\mathrm{NMSE} = 2926$). Gradient flow through $g$ during training is essential.

### 4.3 Penalty Reliability: Convergence and $\lambda$ Sweep

Figure 1(a) shows hard enforcement at $0.00\%$ from epoch 1 while seed 42 under soft $\lambda = 10$ plateaus at $26.1\%$—the gap persists despite 500 epochs of training, independent of training budget. Panels (c–d) show the $\lambda$ sweep (unnormalised MSE; Table 1 uses NMSE per Eq. 5): no $\lambda$ reaches zero violations; at $\lambda = 100$ the mean rate is still $3.7\%$ and MSE is $81\%$ above hard. The violation-vs-$\lambda$ relationship is non-monotonic ($\lambda = 10$ is *worse* than $\lambda = 1$: $6.6\%$ vs. $5.0\%$), reflecting non-monotonic sensitivity to loss landscape geometry. Panels (e–g) show per-seed violations: soft methods span up to 38 pp across seeds; hard collapses to zero; log-param on VDV is simultaneously zero-violation and accurate ($0.272 \pm 0.219$).

## 5 Conclusion

No single inductive bias dominates, but the choice is principled: use hard enforcement for mixed or unknown state structure, log-param for all-concentration states, stoich-param for reaction-explicit systems. Soft penalty methods are unreliable: the training–inference gap produces seed-dependent, $\lambda$-insensitive violations within tested budgets ($\lambda = 1$–$100$, 500 epochs). Hard enforcement is the safe default (0.00% violations everywhere; 99% NMSE reduction on exothermic CSTR) but carries a map-specific accuracy cost (VDV CSTR): softplus hard ($246.5$) is outperformed by ReLU projection ($104.3$, $0.00\%$ violations), approaching unconstrained accuracy (mean $104.3$) while eliminating all violations. Gradient flow through $g$ during training is essential.

**Limitations.** Guarantees hold only at discrete ODE output points; if the RHS requires strict positivity ($\log C$, $1/C$ in kinetics), enforce within solver stages or reparameterise the state. Port-

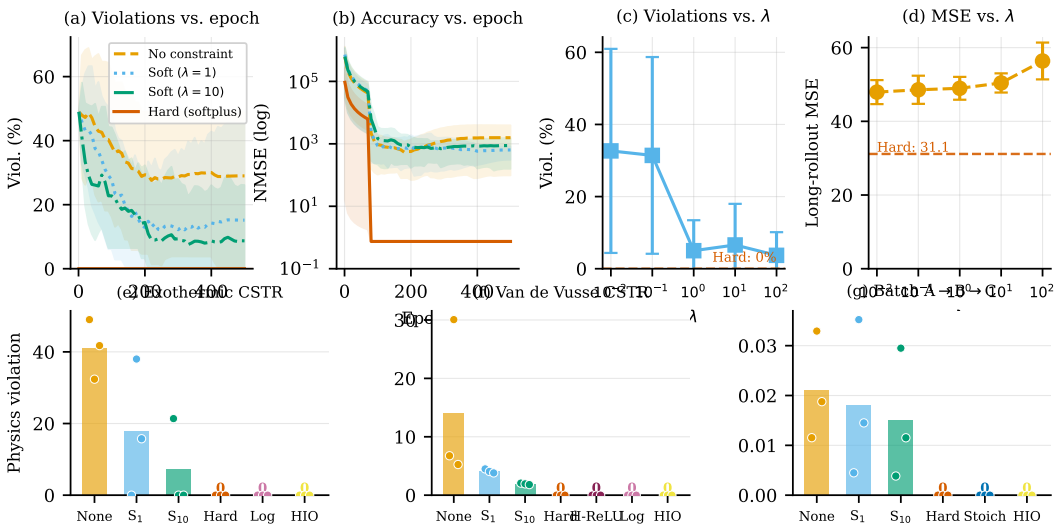


Figure 1: **Top row**: convergence on exothermic CSTR (500 epochs) and soft penalty $\lambda$ sweep. (a) Positivity violation rate vs. epoch: hard (red) is $0.00\%$ from epoch 1; soft seed 42 plateaus at $26.1\%$ even at $\lambda = 10$. (b) NMSE (log scale) vs. epoch; shaded bands: $\min / \max$ across 3 seeds. (c) Violation rate vs. $\lambda$: no $\lambda$ reaches zero; $\lambda = 10$ is non-monotonically *worse* than $\lambda = 1$. (d) Long-rollout MSE vs. $\lambda$ (unnormalised): $\lambda = 100$ costs $81\%$ accuracy above hard (31.1) for still-nonzero violations. **Bottom row**: per-seed physics violations across all three benchmarks (bars = mean; dots = individual seeds). (e–f) positivity violation (%); (g) mass drift (absolute). Soft constraints span up to 38 pp across seeds; hard variants collapse to zero; log-param on VDV is simultaneously zero-violation and accurate ($0.272 \pm 0.219$); hard (softplus) on VDV is reproducibly poor ($246.5 \pm 69.4$).

Hamiltonian and GENERIC constraints are evaluated in soft mode only; hard enforcement for dissipative structures and scaling to industrial PFRs are open.

## Acknowledgments and Disclosure of Funding

Code and data: `https://github.com/ktubhyam/reactor-twin`. Experiments run on Apple M-series CPU.

## References

R. T. Q. Chen, Y. Rubanova, J. Bettencourt, and D. K. Duvenaud. Neural ordinary differential equations. In *Advances in Neural Information Processing Systems*, volume 31, 2018.

M. Cranmer, S. Greydanus, S. Hoyer, P. Battaglia, D. Spergel, and S. Ho. Lagrangian neural networks. *arXiv preprint arXiv:2003.04630*, 2020.

M. Finzi, K. A. Wang, and A. G. Wilson. Simplifying hamiltonian and lagrangian neural networks via explicit constraints. In *Advances in Neural Information Processing Systems*, volume 33, 2020.

S. Greydanus, M. Dzamba, and J. Yosinski. Hamiltonian neural networks. In *Advances in Neural Information Processing Systems*, volume 32, 2019.

P. Kidger. On neural differential equations. *arXiv preprint arXiv:2202.02435*, 2022.

O. Owoyele and P. Pal. ChemNODE: A neural ordinary differential equations framework for efficient chemical kinetic solvers. *Energy and AI*, 7:100118, 2022.

M. Raissi, P. Perdikaris, and G. E. Karniadakis. Physics-informed neural networks: A deep learning framework for solving forward and inverse problems involving nonlinear partial differential equations. *Journal of Computational Physics*, 378:686–707, 2019.

A. Sharma, H. Tann, and O. Owoyele. Phy-ChemNODE: Physics-constrained neural ODE surrogate models for reacting flows. *Combustion Theory and Modelling*, 27(5):714–731, 2023.

J. G. Van de Vusse. Plug flow type reactor versus tank reactor. *Chemical Engineering Science*, 19 (12):994–996, 1964.